Cell Reports, Volume *15*

Supplemental Information

Pak4 Is Required during Epithelial Polarity Remodeling through Regulating AJ Stability and Bazooka Retention at the ZA

Rhian F. Walther, Francisca Nunes de Almeida, Evi Vlassaks, Jemima J. Burden, and Franck Pichaud

Supplementary Figure 1: Apico-basal polarity remodeling in the developing photoreceptor

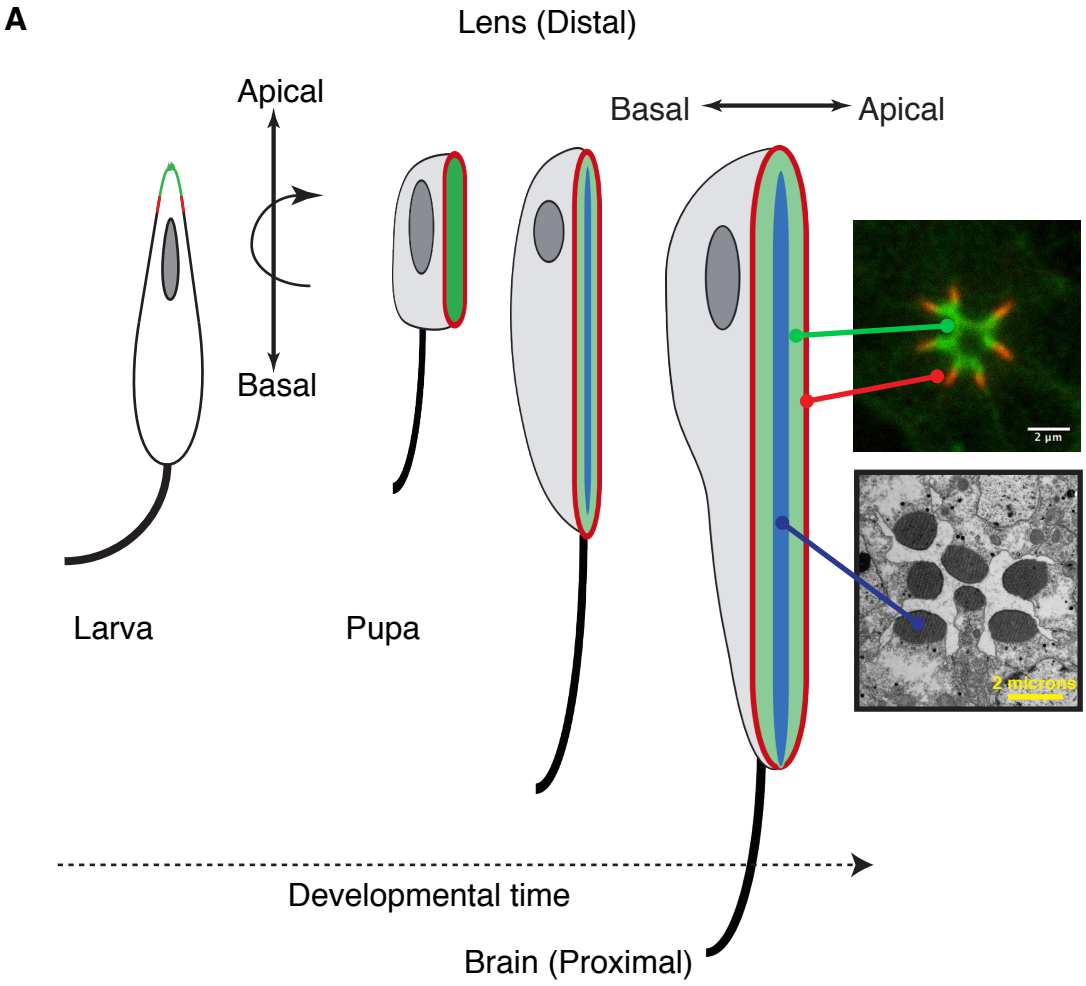

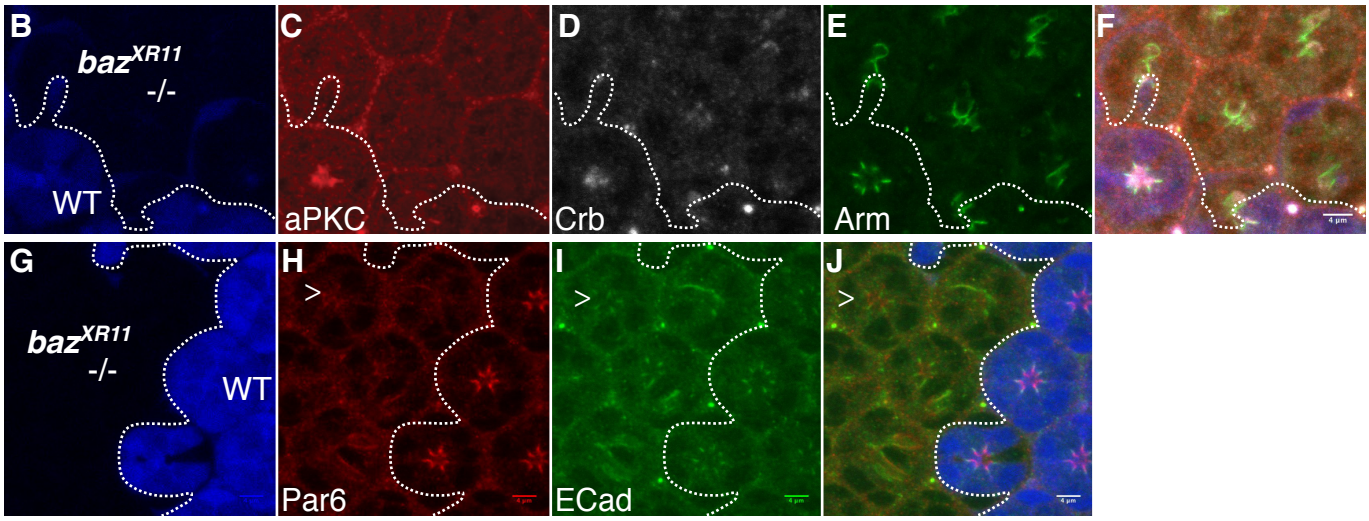

Supplementary Figure 2: *mbt* regulates apical membrane differentiation

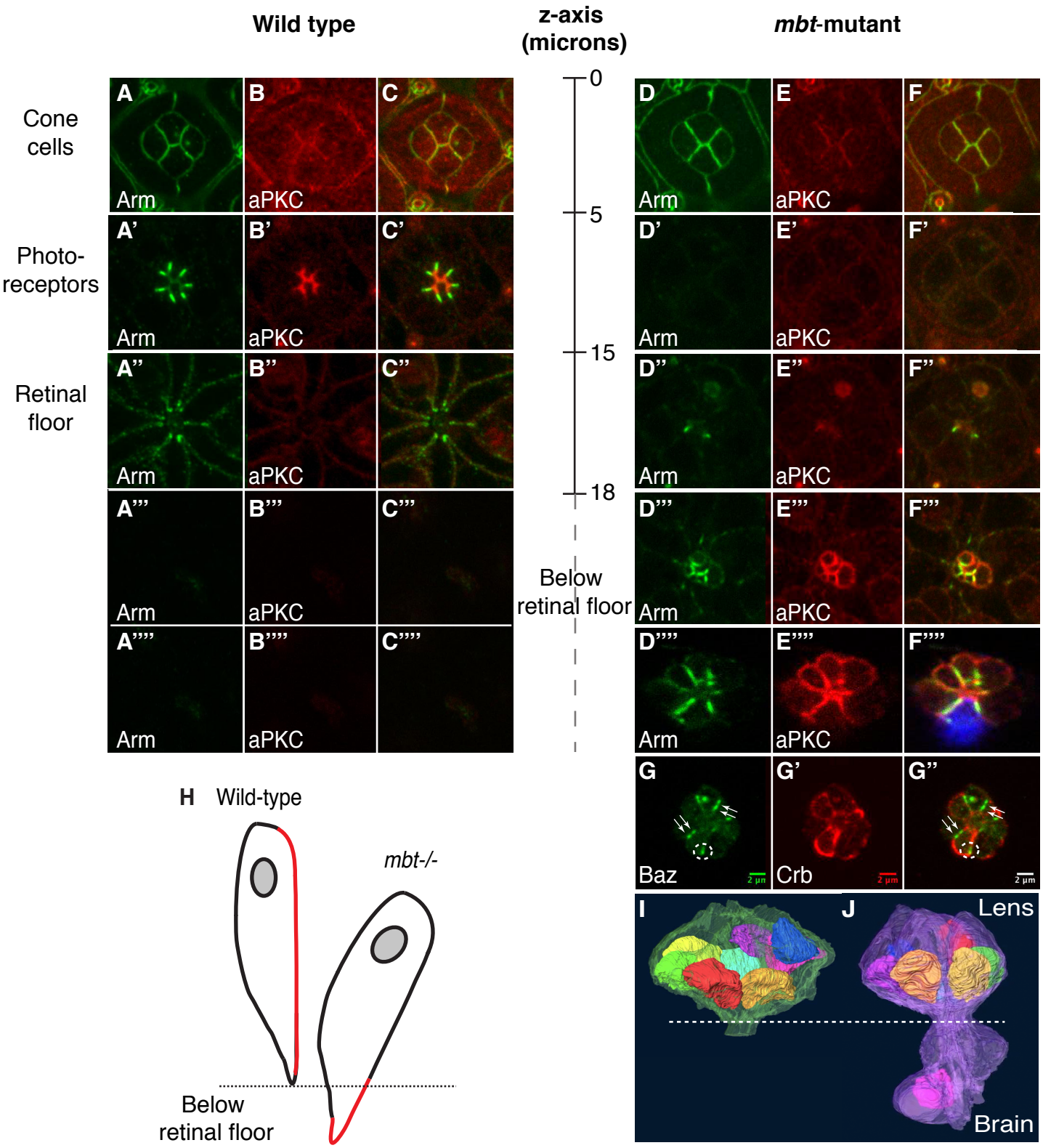

Supplementary Figure 3: Regulated Mbt kinase activity is required during apical membrane differentiation

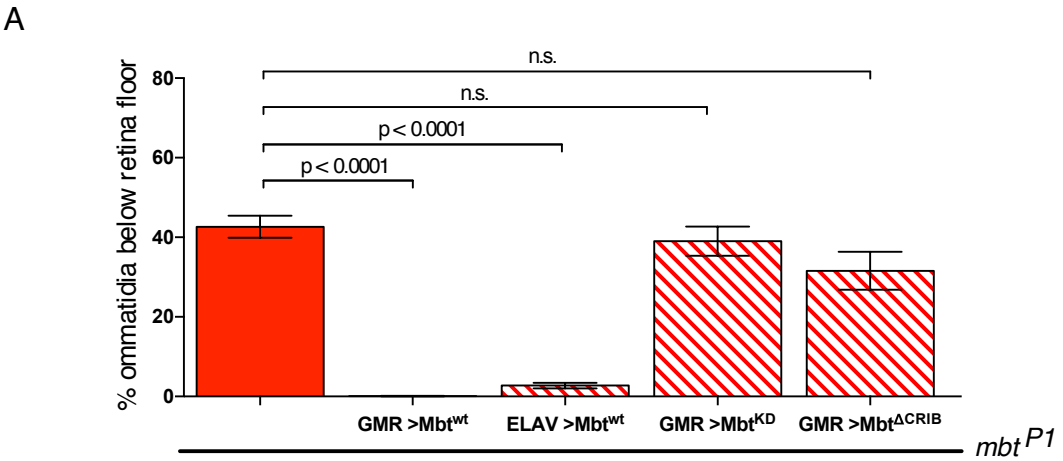

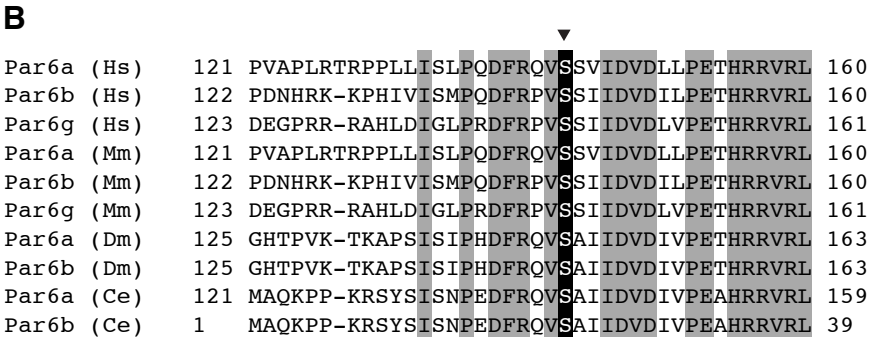

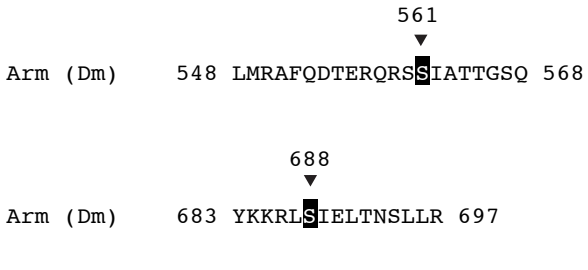

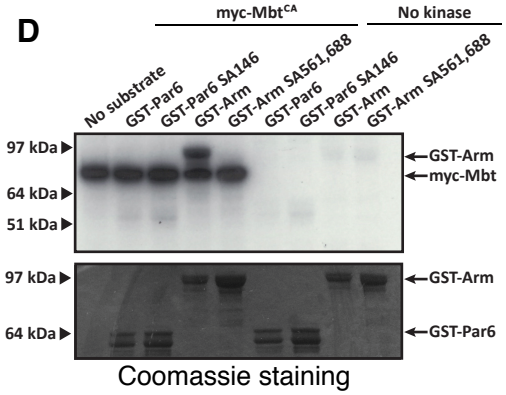

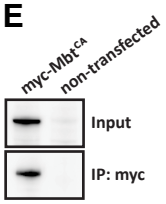

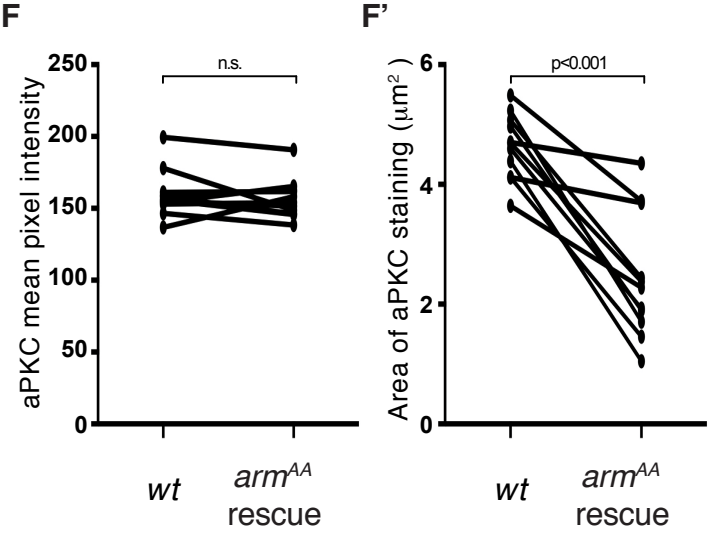

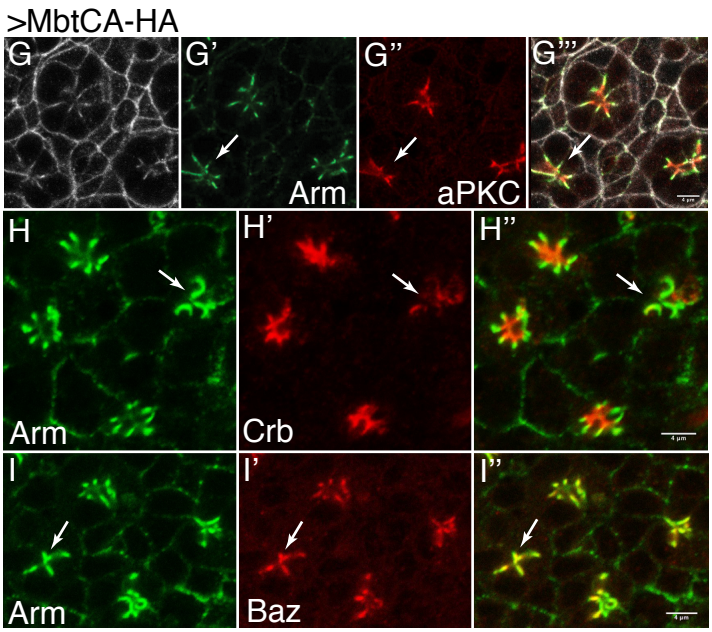

Supplementary Figure 4: Arm phosphorylation regulates *AJ* material stability

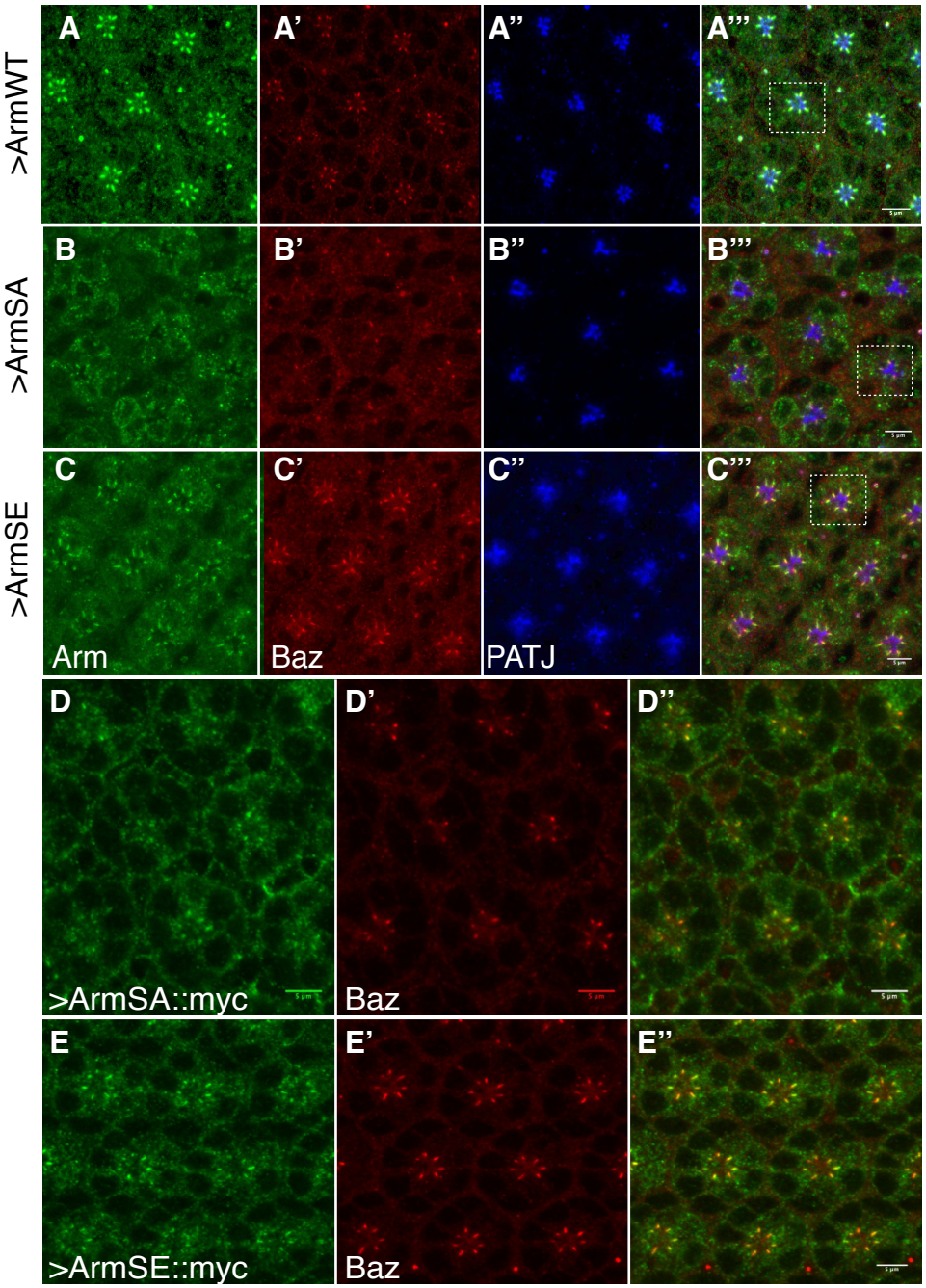

Supplementary Figure 5: Par1 localization and function during photoreceptor morphogenesis

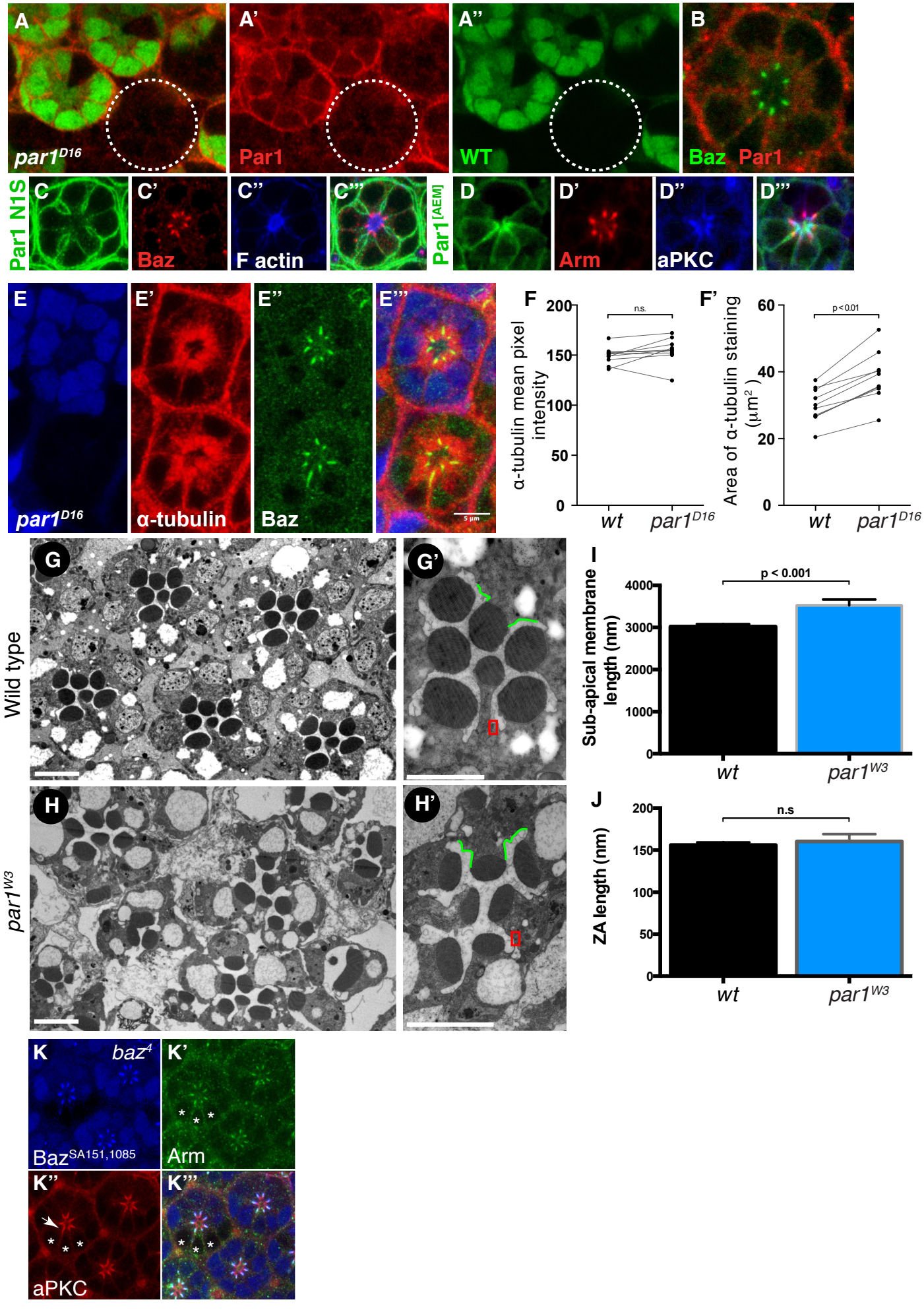

Supplementary Figure 1: Apico-basal polarity remodeling in the developing photoreceptor (A) During pupation, the apico-basal axis of the photoreceptor rotates 90 degrees as the cell undergoes morphogenesis. During pupal development, the new apical membrane domains are subsequently formed over time. *ZA* (red), sub-apical membrane (green) and stack of microvilli (blue). A representative confocal section of a wild type pupal ommatidium and electron micrograph of an adult ommatidum are shown, indicating the respective apical membrane domains. (B-F) baz^{XR11} mutant clone in the pupal retina. Mutant cells lack GFP (blue). aPKC (red), Crb (gray) and Arm (green). (G-J) baz^{XR11} mutant clone in the pupal retina. Par6 (red), E-cadherin (green). A white arrowhead points to residual Par6 staining (H) and *AJ* domains (I). Scale bars = 4 microns.

Supplementary Figure 2: *mbt* regulates apical membrane differentiation (A-F) Series of confocal sections along the lens to brain axis of a wild type ommatidium (A-C) and an mbt^{P1} mutant (D-F). Arm (green), aPKC (red) and merged images are shown in (C-C'''' and F– F''''). (A-F) Cone cell *AJ*. (A'-F') Confocal sections taken at the level of the photoreceptors. (A''-F'') Confocal sections of the retinal floor. In (D'''- F''' and D''''- F'''') consecutive sections below the retina are labeled BRF (Below Retinal Floor). (G-G'') Confocal section of an ommatidium mutant for mbt^{P1} stained for Baz (green) and Crb (red) imaged below the retinal floor. White arrows indicate tandem accumulations of *AJ* material while basally shifted *AJ* material is highlighted by a dashed circle. A merged image is shown in (G''). Scale bars = 2 microns.

(H) Representation of a wild type (left) and *mbt*^{P1} mutant ommatidium (right). The floor of the retina is represented as a dashed line. The apical membrane (i.e sub-apical membrane and *ZA*) is represented as a red line. (I-J) 3D rendering of serial electron microscopy (3View) performed on a wild type (I) and *mbt*^{P1} mutant (J) developing ommatidium at 45% after puparium formation. Photoreceptor nuclei are in solid colors. Cell membranes are in green (wild type) and purple (*mbt*^{P1}). The floor of the retina is highlighted by a dashed white line.

Supplementary Figure 3: Regulated Mbt kinase activity is required during apical membrane differentiation (A) Delamination phenotype in *mbt*^{P1} retina and *mbt*^{P1} expressing the wild type, kinase dead (KD) or ΔCRIB form of Mbt. For each genotype a minimum of 4 retinas were quantified. Columns represent mean and error bars are the SEM of each data set. Statistical significance was determined with one-way ANOVA and Dunnett's multiple comparison test for parametric samples. (B) Alignment of Par6 (Jin et al., 2015). (C) Serine residues 561 and 688 in Arm (Menzel et al., 2008). (D) *In vitro* phosphorylation assay. (E) Myc::Mbt^{CA} was expressed and isolated from S2 cells. (F) Mean pixel intensity of aPKC (F) and aPKC area (F') in paired wild type and *arm*^{3} mutant ommatidia expressing ArmSA561,688::myc. Statistical significance was determined using the Wilcoxon matched pairs test. (G-I) Overexpression of MbtCA (gray). (G') Arm (green) and (G'') aPKC (red). White arrows in G' and G'' indicate an apical domain where no separation of Arm from aPKC occurs. (H) Arm (green) and

(H') Crb (red). (I) Arm (green) and (I') Baz (red). (H-H') A white arrow highlights a poorly differentiated apical domain. (I-I'') A white arrow highlights an ommatidium with defects in apical-basal polarity. Scale bars: 4 microns.

Supplementary Figure 4: Arm phosphorylation regulates *AJ* material stability (A) Overexpression of Arm::myc. In (A-C), Arm (green), Baz (red), PATJ (blue). (B) Overexpression of ArmSA561,688::myc and (C) ArmSE561,688::myc. (D) Overexpression of ArmSA561,688::myc and (E) ArmSE561,688::myc. Myc (green), Baz (red). Scale bars 5 microns.

Supplementary Figure 5: Par1 localization and function during photoreceptor morphogenesis (A-A'') $par1^{D16}$ mutant cells lack nuclear GFP (green). Par1 (red). (B) Par1 (red) and Baz (green). (C-C''') Par-N1S::GFP transgene (green), Baz (red) and F-Actin (blue). (D-D''') Par1-N1S::GFP (AEM) (green), Arm (red) and aPKC (blue). (E-E''') Photoreceptors mutant for $par1^{D16}$ lack nuclear GFP (blue). α-tubulin (red), Baz (green). (F-F') Mean pixel intensity of α-tubulin immunofluorescence (F) and total area of α-tubulin fluorescence (F') in paired wild type and $par1^{D16}$ mutant ommatidia. In (F) and (F'), statistical significance was determined using the Wilcoxon matched pairs test. (G-H) Electron microscopy of a wild type retina (G-G') and a $par1^{W3}$ mutant retina (H-H'). A *ZA* is boxed in red and a sub-apical membrane is highlighted in green in (G') and (H'). Scale bars = 2 microns. (I-J) Length of the sub-apical membrane (I) and *ZA* (J) in wild type and $par1^{W3}$ retina. Columns represent mean and error bars are the SEM of each data set.

(K) *baz*^{4} mutant cells lacking GFP (blue) are highlighted by a white star. The blue channel is also used to show the BazSA151,1085::GFP protein. Arm (green), aPKC (red). A white arrow points to the rescue of aPKC localization.

Fly strains and genetics

The following genotypes were used:

Both the null allele *mbt^{P1} and* hypomorphic allele *mbt^{P3}* (Schneeberger and Raabe, 2003) were used all through this study.

mbt^{P1}FRT19A/FRT19AUbiGFP;eyflp (this work), (Newsome et al., 2000).

w,baz^{4}FRT9.2/ FRT9.2 UbiGFP;*eyflp*. (Nusslein-Volhard et al., 1987).

w,baz^{XR11}FRT19A/ FRT19A UbiGFP;*eyflp* and *w,baz^{EH747}FRT19A/ FRT19A UbiGFP*;*eyflp* (Shahab et al., 2015).

w,baz^{4},sdt^{XP96} FRT9.2/ FRT9.2 UbiGFP;*eyflp* (Muller and Wieschaus, 1996).

mbt^{P1}, baz^{4} FRT9.2/FRT9.2 UbiGFP;eyflp (this work).

w,hsflp;;crb^{11A22}FRT82B/ FRT82B UbiGFP (Tepass et al., 1990); *w, eyflp ; aPKC^{k06403} FRT42D/ FRT42D UbiGFP* (Wodarz et al., 2000). *w,arm^{3} FRT101/FRT101 UbiGFP;eyflp* (Peifer et al., 1991). *w; EGUF, par1^{w3} FRT42D/FRT42D GMR-hid,cl* (Shulman et al., 2000).

eyFLP/+;par1$^{\Delta 16}$FRTG13/FRTG13 UbiGFP. GMR-Gal4/UAS-par1N1S::GFP; GMR-Gal4/UAS-par1::N1S GFP (AEM); (Doerflinger et al., 2007); *GMR-Gal4/UAS-baz::GFP; and bazSA151,1085::GFP* (Benton and St Johnston, 2003). *;GMR-Gal4/ UAS-bazSA151,1085::GFP; mbt^{P1}/Y*; *GMR-Gal4/UAS-baz::GFP;. mbt^{P1}/Y; GMR-Gal4/UAS-bazSA151,1085::GFP;. UAS-mbt^{CA}/CyO; GMR-Gal4/TM2*. (Menzel et al., 2007). *mbt^{P1}/Y; GMR-Gal4/+;UAS-mbt^{WT}/+. mbt^{P1}/Y; ELAV-Gal4/+;UAS-mbt^{WT}/+. mbt^{P1}/Y; GMR-Gal4/UAS-mbt^{CA};. mbt^{P1}/Y*; *GMR-Gal4/+;UAS-mbt$^{\Delta CRIB}$/+* (Menzel et al., 2007). *GMR-Gal4/+; UASt-arm::myc/+* (this work). *GMR-Gal4/+; UASt-armSA561,688::myc/+* (this work). *GMR-Gal4/+ ; UASt-armSE561,688::myc/+* (this work). *w,arm^{3} FRT101/FRT101*

UbiGFP;eyflp/GMR-Gal4; UASt-arm::myc/+;. w,arm^{3} FRT101/FRT101 UbiGFP;eyflp/GMR-Gal4; UASt-armSA561,688::myc/+;. *w,arm^{3} FRT101/FRT101 UbiGFP;eyflp/GMR-Gal4*; *UASt-armSE561,688::myc/+*;. General fly cultures and crosses were carried out at 25^{o}C.

Transgenic flies

Clone LD23131 encoding Armadillo cDNA was obtained from the Drosophila Genomics Resource Center and then subcloned into the pENTR™/D-TOPO® vector (Invitrogen). Residues S561 and S688 were mutated to alanine or glutamic acid using the QuikChange Lightning Multi Site-Directed Mutagenesis Kit. Following sequence verification (MWG Eurofins), the wild-type, SA561,688 and SE561,688 entry clones were used for Gateway cloning (Invitrogen) into the pTWM destination vector (Murphy lab) for expression of a C-terminally Myc tagged protein under the control of the UAST promoter. Injections were performed by BestGene (Chino Hills, CA).

Kinase Assay

GST-tagged Par6, Par6SA146, Arm and ArmSA561,688 were cloned into a pDEST15 vector containing an N-terminal GST tag using the Gateway Cloning System (Invitrogen). Bacteria were lysed by sonication in Lysis Buffer (50 mM Tris HCl pH7.6, 50 mM NaCl, 5 mM $MgCl_2$, 0.5% Triton X-100, 10 mM DTT) in the presence of protease inhibitor (EDTA-free Complete Protease Inhibitor [Roche]). GST fusion proteins were purified using Glutathione Sepharose 4 Fast Flow beads (GE Healthcare) and then washed (50 mM Tris HCl pH 7.4, 50 mM NaF, 300 mM NaCl, 1 % Triton X-100, 1 mM DTT, EDTA-

free Complete Protease inhibitor), eluted (40 mM Glutathione, 50 mM Tris HCl, pH 8.0), and dialyzed against lysis buffer with 40 % glycerol.

Drosophila Schneider S2 cells (DGRC) were transiently transfected with pActin-Myc::Mbt^{CA} (S492N, S521E) and lysed in 50 mM Tris HCl pH 7.5, 150 mM NaCl, 1 % Triton X-100, 5 mM DTT, EDTA). The lysates were incubated with 4 µg of anti-myc agarose beads (Sigma) for 1h at 4°C. The beads were washed with the kinase buffer (20 mM HEPES, pH 7.6, 150 mM NaCl, 20 mM $MgCl_2$, 10 µL/mL phosphatase inhibitor [Sigma], 20 µM ATP). Beads with kinase were split in 20 µL fractions and then mixed with 30 µg of each substrate GST fusion protein as well as 1 µL of [ɣ-^{32}P]-ATP (5 µCi). Each condition was incubated at 30^{o}C for 30 min. The proteins were separated by SDS-PAGE and visualized by autoradiography.

Electron microscopy

Electron microscopy was performed as in (Pinal et al., 2006) using a Tecnai G2 Spirit transmission electron microscope (FEI, The Netherlands) equipped with a Morada CCD camera (Olympus Soft Imaging Systems). Image quantification was performed using iTEM software.

For serial block face scanning electron microscopy, samples were prepared using a combinatorial heavy metal staining protocol involving thiocarbohydrazide, double osmication and *en bloc* Walton's lead aspartate as described by Ellisman and colleagues; http://ncmir.ucsd.edu/sbfsem-

protocol.pdf. Embedded samples were oriented, re-embedded, and regions of interest were identified from 70nm sections examined by TEM. The region of interest was then excised and mounted with cyanoacrylate glue onto specimen pins. These samples were further trimmed before being coated with gold palladium and mounted in the 3View microtome (Gatan, USA). Once aligned, the sample and microtome were returned to the SEM chamber and put under vacuum. The regions of interest on the block face were re-located in the SEM using backscattered electron detection and the imaging and cutting parameters were optimised for each sample. Data sets of 999 sections were collected with section thickness 75-100nm in a Zeiss Sigma FEG-SEM coupled to the Gatan 3View. Data was imported into Amira (VSG, France), where the cells of interest were manually segmented, reconstructed and rendered in 3D.

References

Benton, R., and St Johnston, D. (2003). Drosophila PAR-1 and 14-3-3 inhibit Bazooka/PAR-3 to establish complementary cortical domains in polarized cells. Cell *115*, 691-704.

Menzel, N., Schneeberger, D., and Raabe, T. (2007). The Drosophila p21 activated kinase Mbt regulates the actin cytoskeleton and adherens junctions to control photoreceptor cell morphogenesis. Mech Dev *124*, 78-90.

Muller, H.A., and Wieschaus, E. (1996). armadillo, bazooka, and stardust are critical for early stages in formation of the zonula adherens and maintenance of the polarized blastoderm epithelium in Drosophila. J Cell Biol *134*, 149-163.

Newsome, T.P., Asling, B., and Dickson, B.J. (2000). Analysis of Drosophila photoreceptor axon guidance in eye-specific mosaics. Development *127*, 851-860.

Nusslein-Volhard, C., Frohnhofer, H.G., and Lehmann, R. (1987). Determination of anteroposterior polarity in Drosophila. Science *238*, 1675-1681.

Peifer, M., Rauskolb, C., Williams, M., Riggleman, B., and Wieschaus, E. (1991). The segment polarity gene armadillo interacts with the wingless signaling pathway in both embryonic and adult pattern formation. Development *111*, 1029-1043.

Pinal, N., Goberdhan, D.C., Collinson, L., Fujita, Y., Cox, I.M., Wilson, C., and Pichaud, F. (2006). Regulated and polarized PtdIns(3,4,5)P3 accumulation is essential for apical membrane morphogenesis in photoreceptor epithelial cells. Current biology : CB *16*, 140-149.

Schneeberger, D., and Raabe, T. (2003). Mbt, a Drosophila PAK protein, combines with Cdc42 to regulate photoreceptor cell morphogenesis. Development *130*, 427-437.
Shahab, J., Tiwari, M.D., Honemann-Capito, M., Krahn, M.P., and Wodarz, A. (2015). Bazooka/PAR3 is dispensable for polarity in Drosophila follicular epithelial cells. Biology open *4*, 528-541.
Shulman, J.M., Benton, R., and St Johnston, D. (2000). The Drosophila homolog of C. elegans PAR-1 organizes the oocyte cytoskeleton and directs oskar mRNA localization to the posterior pole. Cell *101*, 377-388.
Tepass, U., Theres, C., and Knust, E. (1990). crumbs encodes an EGF-like protein expressed on apical membranes of Drosophila epithelial cells and required for organization of epithelia. Cell *61*, 787-799.
Wodarz, A., Ramrath, A., Grimm, A., and Knust, E. (2000). Drosophila atypical protein kinase C associates with Bazooka and controls polarity of epithelia and neuroblasts. J Cell Biol *150*, 1361-1374.